JOURNAL OF PROPULSION AND POWER
Vol. 11, No. 2, March–April 1995

Intake Flow Modeling in a Four-Stroke Diesel Using KIVA-3

Randy P. Hessel* and Christopher J. Rutland†
University of Wisconsin–Madison, Madison, Wisconsin 53711

Intake flow for a dual intake valve diesel engine is modeled using moving valves and realistic geometries. The objectives are to show the importance of intake calculations instead of using assumed initial conditions, to supply spray and combustion models with more accurate initial conditions, and to demonstrate the use of multidimensional modeling to studying intake processes. Global simulation parameters are compared with experimental results and show good agreement. The intake process shows a 30% difference in mass flows and average swirl in opposite directions across the two intake valves. The effect of the intake process on the flowfield at the end of compression is examined. Modeling the intake flow results in swirl and turbulence characteristics that are quite different from those obtained by conventional methods in which compression stroke initial conditions are assumed.

Nomenclature

A = average valve open area during intake
k, ε = turbulent kinetic energy and dissipation
U = average intake flow velocity
u_i = Favré-averaged velocity component
ρ = turbulent-averaged density

Introduction

IN typical multidimensional simulations of internal combustion (IC) engines, the calculations begin after intake valve closing. This greatly simplifies the computational domain, since the intake port and valves can be omitted from the model. Grid generation time then takes a smaller percentage of the overall simulation process time. However, starting calculations after intake value closing (IVC) requires assumptions for initial conditions of the mean flow, turbulence, and temperature fields. Because initial conditions are usually not known in detail, simple uniform distributions are often assumed. This can introduce potentially large inaccuracies in engine simulations, because mixing and combustion processes can be strongly dependent on initial conditions.

Omitting intake calculations precludes studies of how intake processes can be used to alter in-cylinder flowfields. Modification of the intake process is a major means by which an engine designer can control engine performance. Control of the intake flow is expected to play an important role as designers seek to obtain better fuel spray characteristics, fuel mixing and mixture preparation, combustion performance, and emissions reductions to meet federal standards.

Early work in multidimensional modeling of intake flows either concentrated on an accurate model of the intake port with no cylinder,[1] or used a simple valve and port geometry with the cylinder.[2] More recently, the amount of reported work in this area has been increasing. Still, many of these have limitations such as steady flows[3,4] or simple valve and port geometry.[5–8]

The goals of the current efforts are to demonstrate the use of multidimensional modeling for intake flow calculations, to show the importance of intake calculations vs assumed initial conditions, and to supply spray and combustion models with more accurate initial conditions. The present simulations use actual geometries of the intake port, moving valves and cylinder of a dual-intake valve diesel engine. Currently, long run times prevent intake design parameter studies. However, even with a few cases, the present results demonstrate the value of intake calculations for better understanding of the influence of intake flows on in-cylinder flowfields. The calculations reveal details of the flow structure and dynamics that are not obtainable with current experimental methods.

Unsteady, three-dimensional calculations starting prior to intake valve opening and proceeding to fuel injection initiation were carried out using a modified version of the KIVA-3 CFD code.[9–11] The KIVA code solves unsteady, compressible, turbulent-reacting flows on finite-volume grids with arbitrarily moving boundaries. Standard k-ε turbulence modeling is used with wall functions (see Appendix). KIVA was developed primarily for IC engine applications and has gone through several revisions since it was first introduced. It uses modern numerical techniques including implicit integration, second-order centrally differenced diffusion terms, and a second-order flux limiting scheme for convection terms. The most recent version of the code, KIVA-3, solves problems on block-structured grids. Thus, complex geometries, such as the intake port and valves, can be represented efficiently. However, KIVA-3 is not set up to automatically simulate intake flows with moving valves, and extended code modifications were required.[12]

Engine Test Facility

The intake calculations were compared with engine experiments.[13] The engine used in this study is a Caterpillar oil test engine (engine type 1Y540). It is a single-cylinder version of Caterpillar's direct-injection, four-stroke, four-valve-per-cylinder, bowl-in-piston 3406 engine. One injection nozzle located on axis injects fuel through six evenly distributed holes into the cylinder. A schematic diagram of the engine test facility is shown in Fig. 1. The inlet standpipe connects the surge tank to the intake port that then connects to the cylinder. Four critical flow orifices in parallel measure average mass flow rate upstream of the tank. In-cylinder pressure is measured by a pressure transducer located in the head. Experimental quantities measured in this study and used for comparison with the numerical simulation were mass flow rate and volume-average in-cylinder pressure. The surge tank pressure and temperature were used for inputs to the computation.

Presented as Paper 93-2952 at the AIAA 24th Fluid Dynamics, Plasmadynamics, and Lasers Conference, Orlando, FL, July 6–9, 1993; received April 2, 1994; revision received July 6, 1994; accepted for publication July 11, 1994.

*Engineer, Engine Research Center; currently at Cummins Engine Co., Columbus, IN 47201.

†Assistant Professor, Department of Mechanical Engineering, Engine Research Center. Member AIAA.

Table 1 Run conditions for the comparison between computation and experiment

	Experiment	Simulation
Engine speed, rpm	1610	1600
IVO, ATDC	−32 deg	−8.5 deg
IVC, ATDC	213 deg	184 deg
Boost pressure, kPa (inflow boundary)	184.1	184.1
Boost temperature, K (inflow boundary)	311	309
Initial and inlet turbulent kinetic energy, m/s^2	Not known	3.7
Initial and inlet turbulent length scale, m	Not known	Minimum of distance to wall or 0.02

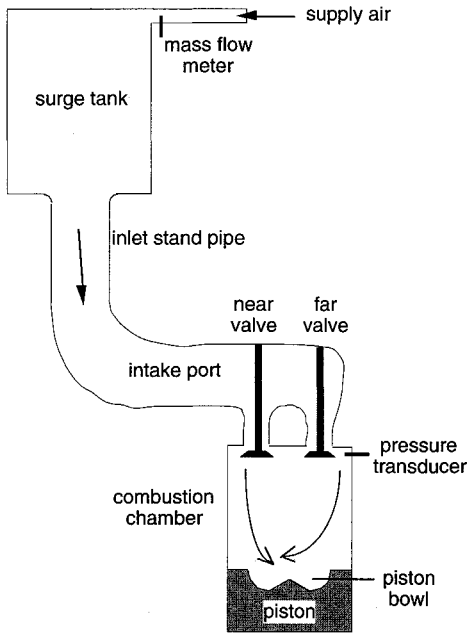

Fig. 1 Schematic of experimental setup. The computational domain includes everything except the surge tank.

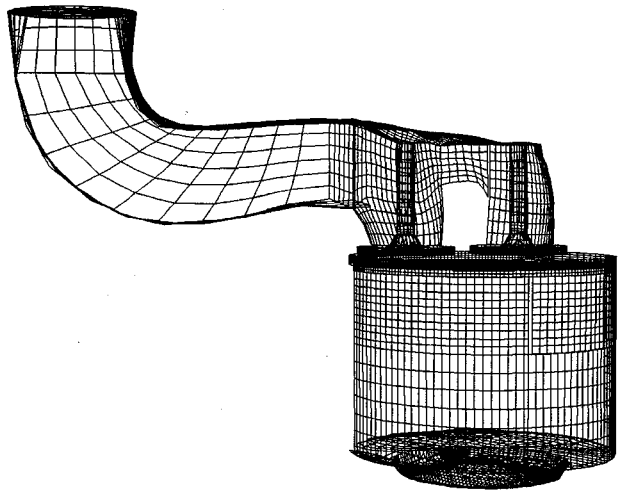

Fig. 2 Surface of the computational grid (stand pipe removed to show detail).

Computational Domain

The computational domain included the inlet stand pipe, the port and valves, and the combustion chamber with the piston bowl, all shown schematically in Fig. 1. The inlet stand pipe-surge tank interface was specified as a constant property (pressure, temperature, turbulence, etc.) boundary. Surge tank measurements support this constant property assumption for pressure and temperature. Including the large inlet stand pipe helps make the calculations less sensitive to inflow boundary conditions.

The simulated intake valves follow the engine's valve lift profile for the majority of the simulation. The "snapping" procedure used by KIVA-3 to move the piston was enhanced to also move the intake valves. Grid snapping is an algorithm for adding or removing grid cells as the grid follows moving boundaries.[11] In KIVA-3, only cells next to a moving boundary change to follow the surface. After a boundary cell volume has changed by ~50% a new cell is added or removed as required (e.g., the grid is snapped), and flow properties are redistributed using mass weighted averaging. This algorithm is efficient and results in no distortion of the solid surfaces in the present calculations. The exhaust valves were not included in the present calculation, but the snapping code enhancements were made general enough to permit exhaust flow modeling for future projects.

The three-dimensional grid was created using a combination of the Gridgen[14] block-structured grid generation software, KIVA-3's preprocessor (K3PREP) and an in-house software package used for grid block manipulation and reshaping. Elliptic grid generation techniques were used so that the local grid point density, grid skewness, orthogonality, and aspect ratios could be adjusted to obtain good quality grids, especially in the complex regions around the valve head (see Rutland et al.[15] for more details). A solid model representation of the computational grid without the standpipe is shown in Fig. 2. Over 120,000 cells were used, which makes the grid density similar to other advanced IC engine calculations.[16]

Typical runs start at −10 deg after top dead center (ATDC) [0 deg = top dead center on intake stroke (TDC)], and continue to the start of fuel injection at 335-deg ATDC. Run times for these cases were 30+ CPU hours on a Cray Y-MP. These long run times are due to the large number of grid points and to the many small cells required by the complex port geometry. For spray and combustion studies in future work, results from full intake calculations at the time of intake valve closure will be interpolated to regular grids of just the combustion chamber. This will significantly reduce computational time. The long run times prevent any serious study of grid density effects. However, four cases, with different operating conditions, were calculated to help check consistency and reasonableness of the results. Since overall trends were similar, only two cases are reported here.

Comparison with Experiment

Computational results were compared to experiments for a fired engine. Table 1 summarizes computational and experimental running conditions. The movement of the valves is realistically simulated by actual movement of the valves in the calculation, and the simulated valve open area is the same as the actual open area. This is accomplished via the snapper algorithm without any distortion of the valve shape. However, to avoid excessively small cells, the initial opening and final closing of the valves is accomplished by adding zero thickness walls around the valve curtain at a lift of 1 mm. Thus, the actual and simulated intake valve opening (IVO) and closing (IVC) times are somewhat different (Table 1). The error in mass flow across the valves introduced by this difference is negligible (see Table 2), since the area is very small and boundary-layer blockage is significant.

Table 2 Comparison of experimental and simulation flow results (also see Fig. 3)

	Experiment	Simulation	Difference
Mass flow rate, kg/min	3.820	3.858	1.0%
Discharge coefficient	Unknown	0.4	——
Pressure at 335 deg, kPa	3201	3472	8.5%

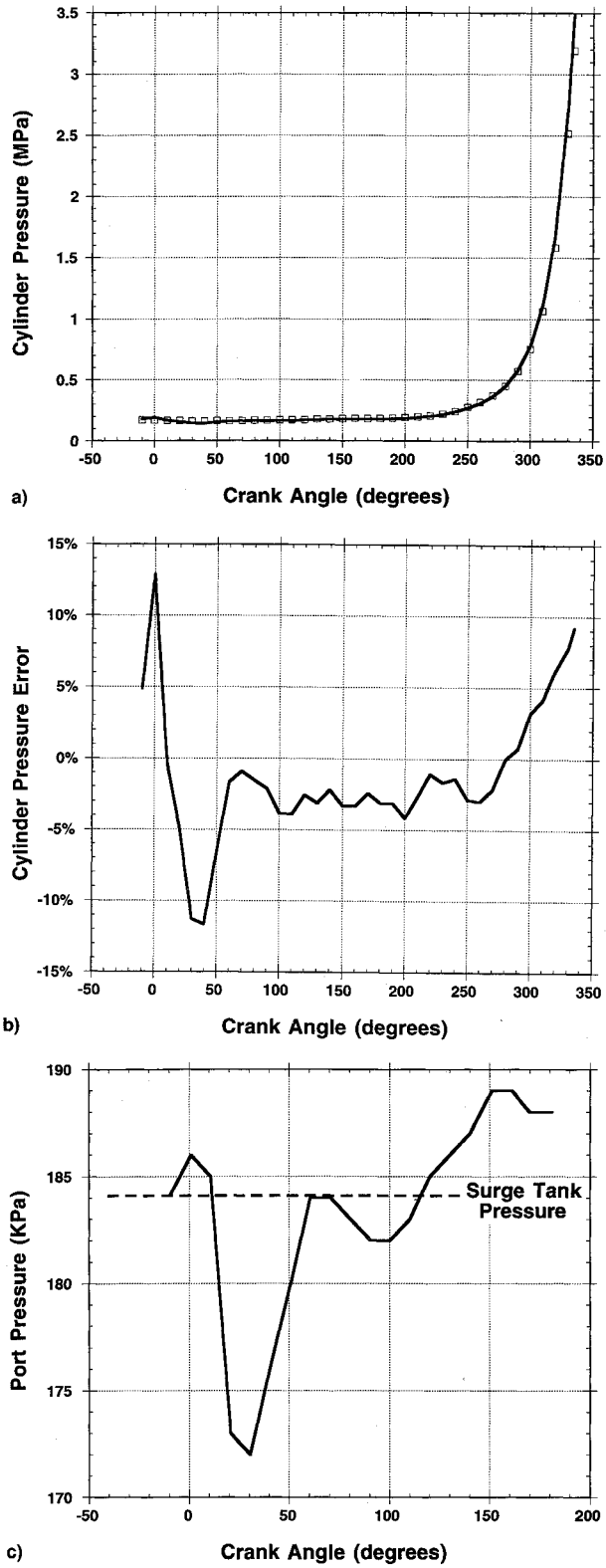

Fig. 3 Volume-averaged cylinder pressure, percent error, and port pressure during intake: a) total cylinder pressure (measured values—symbols, calculated values—line); b) percent error in cylinder pressure (calculated minus measured); and c) port pressure.

Initial air pressure and temperature in the inlet stand pipe and intake port were set equal to surge tank conditions. Initial in-cylinder air pressure was obtained experimentally.[13] Initial air and wall surface temperatures were matched to the same initial data used in a thermodynamic cycle simulation code for the Caterpillar engine. In the multidimensional simulations, all surface temperatures were held constant. A constant pressure boundary is applied at the entrance of the inlet pipe where it attaches to the surge tank.

Table 2 shows a comparison between experimental and calculated results. In-cylinder pressure is volume-averaged over the combustion chamber. Agreement for total mass flow rates is very good, within 1%. This indicates that adjustments made to IVO and IVC times introduced little error, and setting initial port pressure and temperature equal to surge tank conditions is a good approximation. The valve discharge coefficient was very uniform at a value of 0.4 for most of the intake process. The volume-averaged pressure, calculated at the end of the simulation, overpredicts the experimental value by 8.5%. This can be accounted for by several physical effects not modeled in the intake calculation. The exhaust valves are not modeled and there is some overlap with the intake values, as explained below. In addition, blowby, which is the air that escapes from the cylinder by the rings between the piston and cylinder wall, was not modeled. The existing model requires checking with experimental values that are unknown. By not modeling blowby, more mass remains in the cylinder for the simulation than in the experiment, and the simulation pressures are larger.

Volume-average cylinder and port pressures, and percent error as a function of crank angle are shown in Fig. 3. Errors from -10 to 60 deg (Fig. 3b) are caused by not modeling the exhaust valves. The exhaust valves start to close at 33-deg ATDC. In the experiments, this allows some of the flow to escape from the combustion chamber before 0 deg (TDC), resulting in higher calculated mean pressures. From 0 to 33 deg, the piston is moving down and draws air into the cylinder region. In the experiments, some exhaust gases are brought back into the combustion chamber so that the calculations underpredict the average pressure. By 60 deg the exhaust valves are closed, and these errors stabilize and remain constant until approximately 250 deg. At this time the mean pressure begins to rise significantly (Fig. 3a), blowby becomes important, and the calculations without blowby overpredict pressures (Fig. 3b).

Intake Flow Dynamics

Some of the preliminary intake flow characteristics have been reported elsewhere.[15] This included the evolution of volume-averaged turbulence energy and length scale, and average swirl (angular momentum). The results for turbulence quantities were as expected: turbulence parameters increase during intake when the strong intake jets are present, and then decay during compression. Recent results for swirl are somewhat unusual and are discussed in this section.

An important characteristic of IC engine flows is the swirl ratio. This is the spatially averaged vertical component of angular momentum normalized by engine rpm and spatially averaged density. Swirl is often used in diesel engines to help mix the injected liquid fuel. In this report, counterclockwise swirl is positive, and clockwise swirl is negative. The next few paragraphs outline the swirl history during intake and compression processes in terms of the swirl ratio.

Figure 4 shows velocity vectors of interest in the port during the intake stroke at 60-deg ATDC. The valve on the left will be referred to as the "near" valve, as it is nearer to the flow inlet (see Fig. 2). Accordingly, the valve on the right will be called the "far" valve. The computed results show that 30% more air enters the cylinder through the far valve than the near. Figures 2 and 4 help explain this uneven distribution. Notice in Fig. 2 that the port geometry is such that air ap-

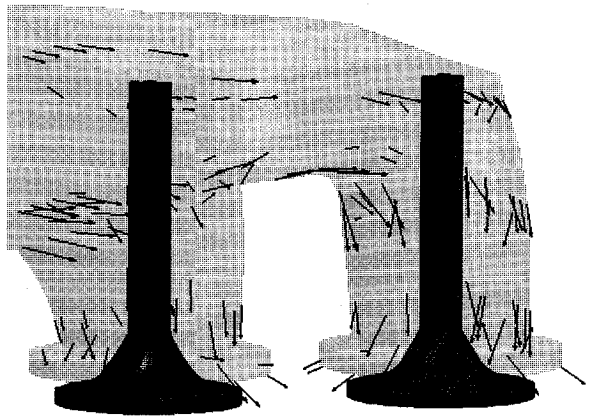

Fig. 4 Representative velocity vectors showing the port flow in the valve vicinity at 60-deg ATDC.

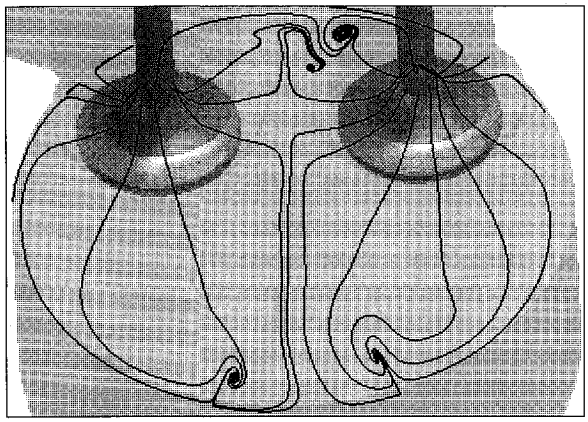

Fig. 5 Instantaneous streamlines originating in the port near each valve at 60-deg ATDC. Streamlines are constrained to lie above a horizontal plane ~4 mm from the head.

proaching the near valve has two paths available. One path leads into the cylinder, the other leads to the far valve. On the other hand, air approaching the far valve is only directed into the cylinder. Concentrating on the near valve, flow at the top of the port has almost no downward velocity component. Vectors at midheight show some of the near valve flow to be directed down toward the cylinder, while a portion is deflected upward and toward the far valve by the port wall.

Figure 5 shows instantaneous particle tracks to visualize the flow as it passes over the valve heads and enters the cylinder at 60-deg ATDC. The particle tracks originate in the port region about the base of the valve stems. Upon entering the cylinder, they are constrained to lie in a plane perpendicular to the cylinder axis and approximately 4 mm from the head. Figure 5 indicates that in the upper part of the chamber there is very little large-scale mixing between the flow streams from each valve. This was maintained during much of the filling process while the valves were open and the piston moved downward. The filling is a rapid process so that turbulent mixing, which is fairly slow, does not significantly enhance the overall mixing. Thus, each valve tends to fill its own side of the cylinder. This was confirmed with streamline flow visualization over the complete volume as well as using streamlines constrained to vertical and horizontal planes. This is important since the port geometry of the CAT engine caused the net swirl generated by each valve's flow to be in opposite directions.[15] Thus, formation of a uniform swirl that fills the complete volume is inhibited. Such uniform swirl is often assumed as initial conditions for in-cylinder simulations.

Turbulence parameters are also typically assigned to be uniformly distributed throughout the cylinder. A commonly used set of empirical correlations for the volume-averaged turbulent kinetic energy and dissipation at IVC are given by[17]

$$k = C_k U^2 \tag{1a}$$

$$\varepsilon = C_\varepsilon (U^3/\sqrt{A}) \tag{1b}$$

Adjusting for the current engine conditions, the recommended values[17] for the constants in Eq. (1) are 0.165 for C_k, and 0.055 for C_ε. Volume-averaging the data in the present intake calculations resulted in 0.230 for C_k and 0.164 for C_ε. Considering the complexity of intake flows and the simplifications inherent in Eq. (1), this agreement is actually fairly good. This further supports the use of this type of correlation when intake calculations are not possible.

Intake Effects on the Flowfield at Start of Fuel Injection

Effects of intake processes on the resulting flowfield just prior to fuel injection are determined by comparing two simulations. One simulation calculates the full intake and compression strokes up to 335-deg ATDC. The other simulation begins near IVC and calculates only the compression stroke using uniform in-cylinder quantities as initial conditions. The latter is common practice for most in-cylinder modeling calculations.

The run that simulates the intake and compression processes is called the INTAKE run, since it uses the full intake calculation. It is very similar to the simulation discussed in the previous section, except it simulates a nonboosted case. Thus, initial port conditions were set equal to the in-cylinder conditions at −10 deg, instead of equal to surge tank conditions. This resulted in a slightly lower mass flow rate and somewhat higher in-cylinder temperatures than the previous simulation.

The INTAKE run was compared to a run called NO-INTAKE. The NO-INTAKE simulation began at a crank angle of 190-deg ATDC (0 deg = TDC intake). By this time the intake valves were closed. The NO-INTAKE run used volume-averaged in-cylinder flow quantities from the INTAKE run at 190 deg as initial conditions. This means that in-cylinder flow characteristics such as density, angular velocity, turbulent kinetic energy, turbulent length scale, etc., were averaged throughout the cylinder when the INTAKE case reached 190 deg. These average values were then assigned to be uniformly distributed throughout the cylinder as initial conditions for the NO-INTAKE run.

Figure 6 compares differences between the INTAKE and NO-INTAKE cases for volume-averaged in-cylinder swirl as

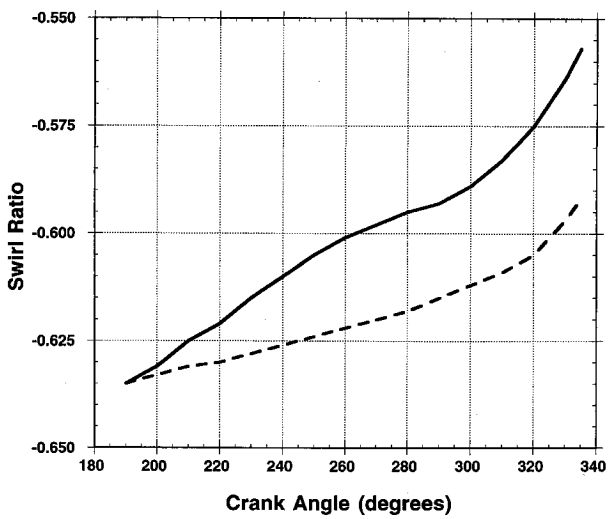

Fig. 6 Comparison of volume-averaged swirl (negative values indicate clockwise). The main point of interest is the change in absolute value (INTAKE case: solid line; NO-INTAKE case: dashed line).

it evolves with crank angle through the compression stroke. The important result in Fig. 6 is that by 335 deg the average in-cylinder swirl magnitude has decreased 13.6% for the INTAKE case, compared to only a 6.7% decrease for the NO-INTAKE case. Even more interesting information is revealed in Fig. 7, which shows planar swirl profiles for both runs, and helps to explain this difference. Planar terms are quantities that are averaged over planes perpendicular to the cylinder axis. This provides a swirl profile along the cylinder axis. Results for four crank angles are shown in Fig. 7. The cylinder head is located at 18.3 cm. The bottom of the bowl is located where swirl goes to zero. The first four nonzero values above this point are in the bowl. The piston face is located between the fourth and fifth data points from the bottom, usually where large changes in swirl occur.

In the NO-INTAKE case (Fig. 7a), swirl is initiated as solid body rotation. Near solid body rotation prevails through to 335 deg, as indicated by the flatness of the swirl profiles. This occurs because there are no grid-resolved, smaller scale structures in the flow, and wall friction is the only effect that diminishes swirl.

Figure 7b shows the swirl history for the INTAKE case during compression. At 220 deg there is negative (clockwise) swirl near the piston and positive (counterclockwise) swirl near the head. This interesting flow configuration is thought to be the result of the intake process discussed in the previous section. In particular, the unequal mass flow and the different swirl directions across the valves could produce this stratified swirl configuration. The far valve has clockwise (negative) swirl and a higher mass flow rate. Also, there is little mixing between the valve flows in the upper part of the chamber during much of the time the valves are open. This permits the higher momentum, negative swirl to reach the bottom of the combustion chamber where it dominates the flow. The upper part of the chamber is then filled by the positive swirl from the near valve.

During the compression stroke, the different rotation directions in the upper and lower parts of the chamber interact and rapidly diminish the volume-average swirl (see also Fig. 6). In addition, in the INTAKE run the flow is not uniform and there are many smaller scale structures resolved on the grid that result from the intake flow. These also act to diminish the large-scale swirl motion.

Swirl that is left at 335 deg, when fuel injection would start, is shown in Fig. 8. The figure shows in-bowl swirl for the NO-INTAKE run to be twice that of the INTAKE run. This implies that the fuel jet sprayed into an intake-generated flowfield is more likely to experience tangential flow velocities half those compared to typical in-cylinder simulations that do not simulate the intake process.

Figure 9 compares values of the total, volume-averaged turbulent kinetic energy for the INTAKE and NO-INTAKE cases. As expected, turbulence is greater for the INTAKE case. The three-dimensional complexity of the intake-generated flow and the more rapid breakdown of the swirl con-

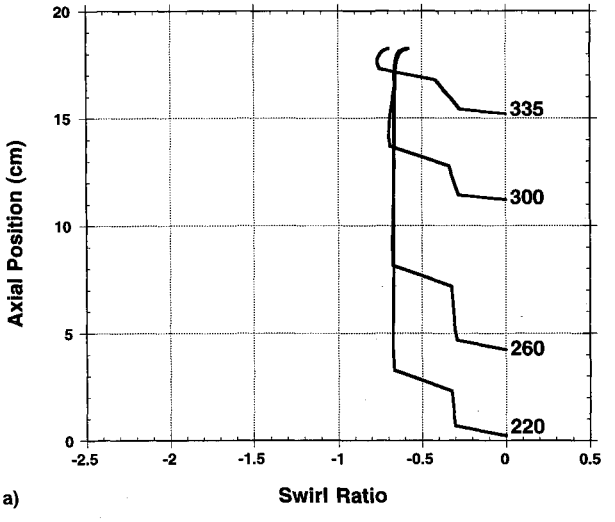

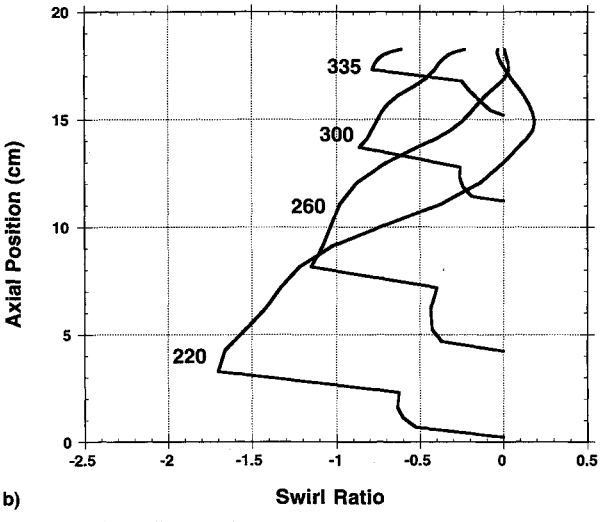

Fig. 7 Swirl profiles during compression: a) NO-INTAKE and b) INTAKE cases. The numbers indicated crank angles of the profiles.

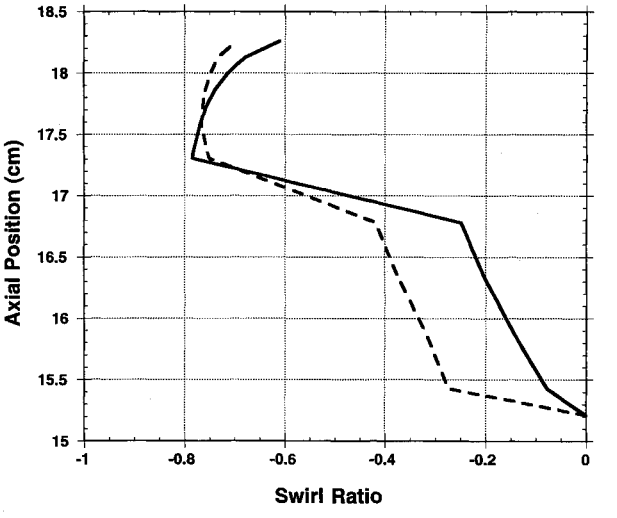

Fig. 8 Swirl profiles at time of fuel injection (INTAKE case—solid line; NO-INTAKE case—dashed line).

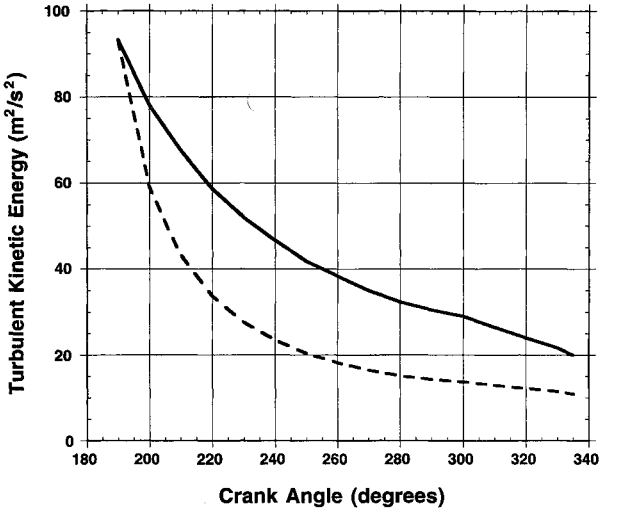

Fig. 9 Comparison of volume-averaged turbulent kinetic energy (INTAKE case—solid line; NO-INTAKE case—dashed line).

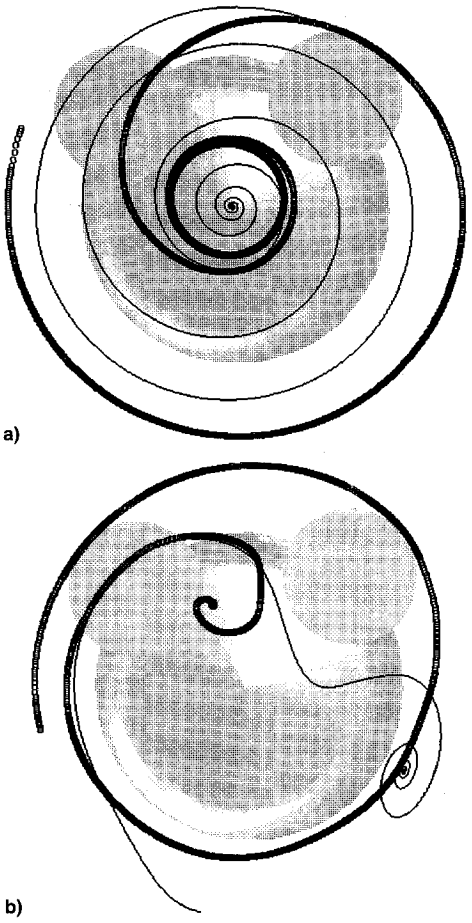

Fig. 10 Horizontal instantaneous streamlines at crank angles 300 deg (thin lines) and 330 deg (thick lines): a) NO-INTAKE and b) INTAKE cases.

tribute to higher turbulence values. Indications are that it is differences in the horizontal velocity components, rather than the vertical component, that contribute to the differences in swirl breakdown and turbulence generation. Some of this can be visualized using streamlines constrained to lie in horizontal planes.

Horizontal instantaneous streamlines for a plane at a fixed distance from the head, but outside the bowl, are plotted in Fig. 10. This shows representative streamlines at two crank angles. The thin streamline is at a crank angle of 300 deg and the thick line is at 330 deg. The two small shaded circles indicate valve positions. The large shaded circle represents the bowl, which is behind the streamlines, but moving towards them as the crank angle increases. For the NO-INTAKE case (Fig. 10a), the change in flow pattern between the two crank angles is very smooth and orderly. This indicates less breakdown of large-scale motion into turbulence. However, for the INTAKE case (Fig. 10b), there is a large change in the flow pattern between the two crank angles, which contributes to increased turbulence generation. These results are also shown by vertical profiles of turbulent kinetic energy averaged on horizontal planes at the time of fuel injection (Fig. 11). Inside the bowl, turbulence levels for the INTAKE case are roughly twice that of the NO-INTAKE run.

Conclusions

Simulations of intake flow processes with the modified KIVA-3 program compare well with global experimental results. Flowfields at the time of fuel injection resulting from intake modeling show notable differences when compared to traditional methods of in-cylinder modeling. The differences in swirl profiles (Fig. 8) and turbulence profiles (Fig. 11) indicate

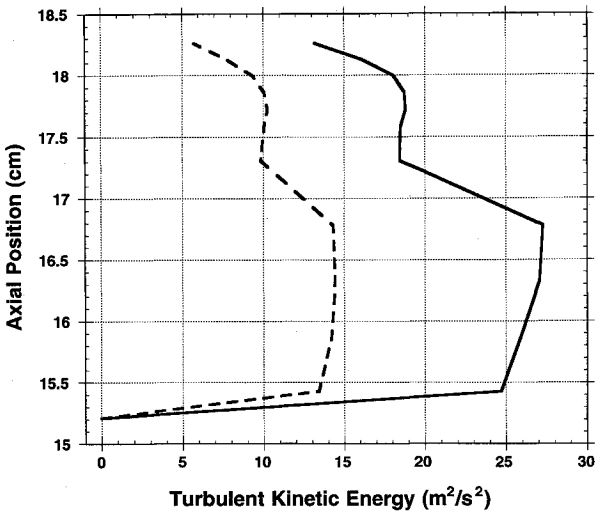

Fig. 11 Profiles of turbulent kinetic energy averaged over horizontal planes at time of fuel injection (INTAKE case—solid line; NO-INTAKE case—dashed line).

a richer flow structure as a result of calculating the full intake flow process. Preliminary results also indicate that this difference will have an important influence on the fuel-air mixing during the fuel injection process. This in turn will have a major influence on how accurately combustion and emissions processes can be predicted with simulations.

Appendix: k-ε Turbulence Model

The k-ε turbulence modeling used in KIVA-3 is fairly standard,[9] with simple extensions for compressibility. Wall functions[9] are used at solid boundaries, and k-ε are specified at inflow boundaries (see Table 1). The equations for k and ε, in tensor notation are given by

$$\frac{\partial \rho k}{\partial t} + \frac{\partial \rho k u_i}{\partial x_i} = \sigma_{ij}\frac{\partial u_i}{\partial x_j} - \frac{2}{3}\rho k\frac{\partial u_i}{\partial x_i} + \frac{\partial}{\partial x_i}\left[\left(\frac{\mu_t}{Pr_k}\right)\frac{\partial k}{\partial x_i}\right] - \rho\varepsilon \tag{A1}$$

$$\frac{\partial \rho \varepsilon}{\partial t} + \frac{\partial \rho \varepsilon u_i}{\partial x_i} = -\left(\frac{2}{3}C_{\varepsilon 1} - C_{\varepsilon 3}\right)\rho\varepsilon\frac{\partial u_i}{\partial x_i} + \frac{\partial}{\partial x_i}\left[\left(\frac{\mu_t}{Pr_\varepsilon}\right)\frac{\partial \varepsilon}{\partial x_i}\right] + \frac{\varepsilon}{k}\left(C_{\varepsilon 1}\sigma_{ij}\frac{\partial u_i}{\partial x_j} - C_{\varepsilon 2}\rho\varepsilon\right) \tag{A2}$$

where all terms are turbulent-averaged quantities with velocities k and ε being Favré-averaged. Other terms and constants are

$$\sigma_{ij} = \mu_t\left(\frac{\partial u_i}{\partial x_j} + \frac{\partial u_j}{\partial x_i} - \frac{2}{3}\frac{\partial u_k}{\partial x_k}\delta_{ij}\right) \tag{A3}$$

$$\mu_t = C_\mu \rho(k^2/\varepsilon) \tag{A4}$$

$$C_{\varepsilon 1} = 1.44 \qquad C_\mu = 0.09$$
$$C_{\varepsilon 2} = 1.92 \qquad Pr_k = 1.0 \tag{A5}$$
$$C_{\varepsilon 3} = -1.0 \qquad Pr_\varepsilon = 1.3$$

Acknowledgments

Support for this work was provided by NASA Lewis Grant NAG-3-1087, W. T. Wintucky contract monitor. Additional support was provided by Caterpillar, Cray Research, the Wisconsin Graduate School, and the Engine Research Center

(Army Research Office Contract DAAL03-86-K-0174). We also acknowledge the help and contributions of Rolf Reitz and Dan Nehmer.

References

[1]Isshiki, Y., Shimamoto, Y., and Wakisaka, T., "Numerical Prediction of Effect of Intake Port Configurations on the Induction Swirl Intensity by Three-Dimensional Gas Flow Analysis," Comodia Conference Proceedings: *Diagnostics and Modeling of Combustion in Reciprocating Engines*, Tokyo, Japanese Society of Automotive Engineering, 1985, pp. 295–304.

[2]Taghavi, R., and Dupont, A., "Investigation of the Effect of Inlet Port on the Flow in a Combustion Chamber Using Multi-Dimensional Modeling," *Journal of Engineering for Gas Turbines and Power*, Vol. 111, No. 7, 1989, pp. 113–121.

[3]Luo, K. H., and Bray, K. N. C., "3D Simulation of Induction Port Flow of a Four-Valve Engine Configuration," Society of Automotive Engineers Paper 920586, 1992.

[4]Aita, S., Tabbal, A., Munck, G., Fujiwara, K., Hongoh, H., Tamura, E., and Obana, S., "Numerical Simulation of Port-Valve-Cylinder Flow in Reciprocating Engines," Society of Automotive Engineers Paper 900820, 1990.

[5]Le Coz, J.-F., Henriot, S., and Pinchon, P., "An Experimental and Computational Analysis of the Flow Field in a Four-Valve Spark Ignition Engine—Focus on Cycle-Resolved Turbulence," Society of Automotive Engineers Paper 900056, 1990.

[6]Sugiura, S., Yamada, T., Inoue, T., Morinishi, K., and Satofuka, N., "Numerical Analysis of Flow in the Induction System of an Internal Combustion Engine—Multi-Dimensional Calculation Using a New Method of Lines," Society of Automotive Engineers Paper 900255, 1990.

[7]Haworth, D. C., El Tahry, S. H., Huebler, M. S., and Chang, S., "Multidimensional Port-and-Cylinder Flow Calculations for Two- and Four-Valve-Per-Cylinder Engines: Influence of Intake Configuration on Flow Structure," Society of Automotive Engineers Paper 900257, 1990.

[8]Kuo, T.-W., "Multidimensional Port-and-Cylinder Gas Flow, Fuel Spray, and Combustion Calculations for a Port-Fuel-Injection Engine," Society of Automotive Engineers Paper 920515, 1992.

[9]O'Rourke, P. J., Amsden, A. A., Butler, T. D., and McKinley, T. L., *Improvements of the KIVA-II Computer Program for Numerical Combustion*, Los Alamos Rept. LA-11560-MS, 1989.

[10]Amsden, A. A., O'Rourke, P. J., Butler, T. D., Meintjes, K., and Fansler, T. D., "Comparisons of Computed and Measured Three-Dimensional Velocity Fields in a Motored Two-Stroke Engine," Society of Automotive Engineers Paper 920418, 1992.

[11]Amsden, A. A., *KIVA-3: A KIVA Program with Block-Structured Mesh for Complex Geometries*, Los Alamos National Lab., LA-12503-MS, 1993.

[12]Hessel, R. P., "Numerical Simulation of Valved Intake Port and In-Cylinder Flows Using KIVA-3," Ph.D. Dissertation, Dept. of Mechanical Engineering, Univ. of Wisconsin–Madison, Madison, WI, 1993.

[13]Nehmer, D. A., "Measurement of the Effect of Injection Rate and Split Injections on Diesel Engine Soot and NOx Emissions," Dept. of Mechanical Engineering, M.S. Thesis, Univ. of Wisconsin–Madison, Madison, WI, 1993.

[14]Steinbrenner, J. P., Chawner, J. P., and Fouts, C. L., *The GridGen 3D Multiple Block Grid Generation System, Volume II: User's Manual*, Vol. II, Flight Dynamics Directorate, Wright Lab., WRDC-TR-90-3022, April 1991.

[15]Rutland, C. J., Pieper, C. M., and Hessel, R., "Intake and Cylinder Flow Modeling with a Dual-Valve Port," Society of Automotive Engineers Paper 930069, 1993.

[16]El Tahry, S. H., and Haworth, D. C., "Directions in Turbulence Modeling for In-Cylinder Flows in Reciprocating Engines," *Journal of Propulsion and Power*, Vol. 8, No. 5, 1992, pp. 1040–1048.

[17]Grasso, F., Wey, M. J., Bracco, F. V., and Abraham, J., "Three-Dimensional Computations of Flows in a Stratified-Charge Rotary Engine," Society of Automotive Engineers Paper 870409, 1987.